ASTROCAM:
An Offner Re-imaging 1024 x 1024 InSb Camera
for Near-Infrared Astrometry on the USNO 1.55-m Telescope

Jacqueline Fischer*[a], Frederick Vrba[b], Douglas Toomey[c], Robert Lucke[a], Shu-i Wang[d],
Arne Henden[b,e], Joseph Robichaud[f], Peter Onaka[g], Brian Hicks[a], Fred Harris[b],
Werner Stahlberger[h], Kris Kosakowski[f], C. C. Dudley[a] and Kenneth Johnston[i]

[a]Naval Research Laboratory, Remote Sensing Division, Washington, DC, USA
[b]U.S. Naval Observatory, Flagstaff Station, PO Box 1149, Flagstaff, AZ, USA
[c]Mauna Kea Infrared, LLC, 159 Kalanikoa St, Hilo, HI USA
[d]University of Chicago Engineering Center, 5640 S Ellis Ave, Chicago, IL, USA
[e]Universities Space Research Association, USA
[f]SSG Precision Optronics, Inc., 65 Jonspin Rd, Wilmington, MA, USA
[g]Applied Designs, 3001 Specific Heights Rd, Honolulu, HI, USA
[h]CAD Services, 1158 Mowai St, Kailua, HI, USA
[i]U.S. Naval Observatory, 3450 Massachusetts Ave NW, Washington, DC, USA

ABSTRACT

In order to extend the US Naval Observatory (USNO) small-angle astrometric capabilities to near infrared wavelengths we have designed and manufactured a 1024 x 1024 InSb re-imaging infrared camera equipped with an array selected from the InSb ALADDIN (Advanced Large Area Detector Development in InSb) development program and broadband and narrowband 0.8 - 3.8 μm filters. Since the USNO 1.55-m telescope is optimized for observations at visible wavelengths with an oversized secondary mirror and sky baffles, the straylight rejection capabilities of the ASTROCAM Lyot stop and baffles are of critical importance for its sensitivity and flat-fielding capabilities. An Offner relay was chosen for the heart of the system and was manufactured from the same melt of aluminum alloy to ensure homologous contraction from room temperature to 77 K. A blackened cone was installed behind the undersized hole (the Lyot stop) in the Offner secondary. With low distortion, a well-sampled point spread function, and a large field of view, the system is well suited for astrometry. It is telecentric, so any defocus will not result in a change of image scale. The DSP-based electronics allow readout of the entire array with double-correlated sampling in 0.19 seconds, but shorter readout is possible with single sampling or by reading out only small numbers of subarrays. In this paper we report on the optical, mechanical, and electronic design of the system and present images and results on the sensitivity and astrometric stability obtained with the system, now operating routinely at the 1.55-m telescope with a science-grade ALADDIN array.

Keywords: Infrared imaging; astrometry; optical design; infrared array electronics

1. INTRODUCTION

Until recently, the majority of parallax measurements of distances to nearby stars have been carried out in the visible band using direct imaging on large format charge coupled devices (CCDs). Typical parallax measurements in the optical, carried out by observing the object field periodically during the Earth's annual orbit around the Sun and, following standard data reduction procedures such as flat-fielding and calibration, centroiding of the object with respect to the field stars in the image, provide determination of the parallax to within 1 or 2

---

*Correspondence: 4555 Overlook Ave SW, Washington DC 20375 USA, Jackie.Fischer@nrl.navy.mil, 1 202 767 3058

			Form Approved
	Report Documentation Page		OMB No. 0704-0188

Public reporting burden for the collection of information is estimated to average 1 hour per response, including the time for reviewing instructions, searching existing data sources, gathering and maintaining the data needed, and completing and reviewing the collection of information. Send comments regarding this burden estimate or any other aspect of this collection of information, including suggestions for reducing this burden, to Washington Headquarters Services, Directorate for Information Operations and Reports, 1215 Jefferson Davis Highway, Suite 1204, Arlington VA 22202-4302. Respondents should be aware that notwithstanding any other provision of law, no person shall be subject to a penalty for failing to comply with a collection of information if it does not display a currently valid OMB control number.

1. REPORT DATE **2003**	2. REPORT TYPE	3. DATES COVERED **00-00-2003 to 00-00-2003**

4. TITLE AND SUBTITLE	5a. CONTRACT NUMBER
ASTROCAM: An Offner Re-imaging 1024 x 1024 InSb Camera for Near-Infrared Astrometry on the USNO 1.55-m Telescope	5b. GRANT NUMBER
	5c. PROGRAM ELEMENT NUMBER
6. AUTHOR(S)	5d. PROJECT NUMBER
	5e. TASK NUMBER
	5f. WORK UNIT NUMBER

7. PERFORMING ORGANIZATION NAME(S) AND ADDRESS(ES) **Naval Research Laboratory,Remote Sensing Division,4555 Overlook Avenue, SW,Washington,DC,20375**	8. PERFORMING ORGANIZATION REPORT NUMBER
9. SPONSORING/MONITORING AGENCY NAME(S) AND ADDRESS(ES)	10. SPONSOR/MONITOR'S ACRONYM(S)
	11. SPONSOR/MONITOR'S REPORT NUMBER(S)

12. DISTRIBUTION/AVAILABILITY STATEMENT
Approved for public release; distribution unlimited

13. SUPPLEMENTARY NOTES
The original document contains color images.

14. ABSTRACT

15. SUBJECT TERMS

16. SECURITY CLASSIFICATION OF:			17. LIMITATION OF ABSTRACT	18. NUMBER OF PAGES **14**	19a. NAME OF RESPONSIBLE PERSON
a. REPORT **unclassified**	b. ABSTRACT **unclassified**	c. THIS PAGE **unclassified**			

Standard Form 298 (Rev. 8-98)
Prescribed by ANSI Std Z39-18

milli-arcseconds.[1,2] By combining results taken over many years, precision as high as 0.5 milli-arcseconds has been obtained for a subset of objects. Of key importance to the attainment of these high precision results is the existence of large format arrays so that a sufficient number of background stars are included in a single image, while still maintaining a well-sampled point spread function. To provide a platform for long-term astrometric programs, the stability of all aspects of the observing system is paramount.

In order to extend the US Naval Observatory (USNO) small-angle astrometric capabilities to near infrared wavelengths and to investigate the precision and flux limits to which astrometry and photometry can be carried out at the USNO 1.55-m telescope, programs to develop large format InSb arrays and to design and construct a camera to house such an array were initiated. In a collaboration between USNO, the National Optical Astronomy Observatories (NOAO), and the Hughes Santa Barbara Research Corporation/Raytheon, the Advanced Large Area Detector Development in InSb (ALADDIN) program developed 1024 × 1024 InSb arrays for astronomy, for which only 256 × 256 arrays were previously available. This paper presents the results of a collaborative program between the Naval Research Laboratory (NRL), USNO, and Mauna Kea Infrared and its subcontractors to design, construct and install on the USNO 1.55-m telescope, ASTROCAM, a 1024 × 1024 InSb re-imaging infrared camera equipped with an array selected from the ALADDIN development program and to verify its capabilities to carry out astrometric and astronomical observations. Since the USNO 1.55-m telescope is optimized for observations at visible wavelengths, with an oversized secondary mirror and sky baffles, the straylight rejection capabilities of the ASTROCAM cold-Lyot stop and baffles were of critical importance for its sensitivity and flat-fielding capabilities.

A camera with the simultaneous attributes of a large field of view and a well-sampled point spread function is optimally suited to measure stellar parallax motions, as well as other time-dependent phenomenon. In this paper we report on the criteria, goals, and solutions that were used in the design of ASTROCAM and on the extent to which they were achieved. Imaging observations that illustrate its capabilities are also presented.

2. THE DETECTOR ARRAY

ASTROCAM houses a science grade ALADDIN array. We briefly summarize the design performance of the array in Table 1 and refer the reader to Fowler et al.[3] for further details.

Table 1. The ALADDIN 1024 × 1024 SBRC InSb Array Performance[3]

Architecture	Four fully independent 512 × 512 quadrants
Pixel size	27 μm square
Effective fill factor	100%
Outputs	32 (8 per quadrant)
Frame Rate	20 Hz
Reset options	Destructive and non-destructive by rows
Full Well	3×10^5 electrons at 1.0 V bias
Wavelength Range	0.8 - 5+ μm with AR coating
Quantum Efficiency	> 80% 0.9 - 5 μm with AR coating
Operating Temperature	30 K
Dark Current	< 0.1 electrons/second
Read noise	25 electrons RMS with Fowler sampling

# 3. THE OPTICAL SYSTEM

3.1. Design criteria

For thermal infrared observations, re-imaging optics are required to provide a cold pupil to enable fabrication of a Lyot stop whose function is to prevent all photons but those emanating from the telescope mirror surfaces from reaching the detector. An all-reflecting optical system is ideal because it is achromatic, has maximal throughput, and does not suffer from "ghosts" associated with multiple reflections from the surfaces of transmissive optical elements. Our choice of an Offner relay (Sect. 3.2) with its unit magnification was based on considerations of point spread function sampling, its zero third-order aberrations, low distortion, telecentricity, and the availability of its secondary as a natural place for a Lyot stop. In the last few years, a number of cameras have utilized Offner re-imaging systems for these and other reasons.[4, 5] In ASTROCAM, the only transmissive elements are the cryostat window and the filters.

The USNO 1.55-m telescope was designed specifically for astrometry at optical wavelengths. Its optical prescription is Newtonian (f/10 paraboloidal primary mirror, flat secondary), but its form is Cassegrainian: the focal point is located behind the primary. This design choice, which implies a large obscuration ratio (0.6) and uncorrected coma, was motivated by a desire to avoid plate scale changes as temperature changes alter the primary-secondary separation. Another advantage of the design is that it has zero Seidel distortion when the primary serves as the entrance pupil. When ASTROCAM is attached, the entrance pupil is an image of ASTROCAM's Lyot stop. This image does not coincide exactly with the telescope's primary, but distortion remains extremely low. The large central obscuration means that only about 40% (compared to the more familiar 84% for an unobscured aperture) of the light from a point source falls within the Airy disc, which has diameter $\approx 19\lambda$ and $\text{FWHM}_{diffraction} \approx 8\lambda$. The effect of coma is to alter the centroid positions of the stellar images,[6] but the effect is small and linear in field angle; at the corner of the field of view it is about the width of an ALADDIN pixel (27 μm = 0.37 arcsec). It therefore appears only as a slight change in plate scale, which is accounted for in calibration and is transparent to the user. The contribution of coma to the FWHM at the corner of the field of view is ≈ 20 μm, which is small compared with the combined seeing and diffraction FWHM discussed next.

A study of seeing statistics on the USNO 1.55-m telescope[7] gave mean, median, and mode zenith seeing at 7000 Å of 1.6, 1.3, and 1.0 arcsec FWHM, respectively, with a minimum of about 0.65 arcsec, attributed to mostly "local" seeing of about 0.57 arcsec that is not wavelength dependent. Diffraction effects become noticeable longward of 3 μm. Assuming optimistically that the mode of non-local seeing scales as $\lambda^{-6/5}$, and adding local and non-local modal seeing FWHMs in quadrature with $\text{FWHM}_{diffraction}$ yields 63.2, 48.9, and 52.5 μm at J(1.25 μm), K'(2.1 μm), and L'(3.8 μm) bands, respectively. Thus the 1:1 magnification provides nearly Nyquist sampling under most zenith seeing conditions for the 27 μm $\times$ 27 μm ALADDIN pixels while providing a 6.2 arcmin $\times$ 6.2 arcmin field of view.

3.2. The Offner re-imager optics design

An Offner reimaging system consists of a pair of spherical mirrors concentric about their centers of curvature: a concave primary M_1 and a convex secondary M_2 with a radius of curvature half of that of the primary. It can be used as we have in ASTROCAM (Fig. 1) to image a field in the plane containing the common center of the mirrors and perpendicular to the optical axis. Such a configuration has unit magnification, is free from third order aberrations, and its primary aberration is fifth-order astigmatism (Offner[8]). In our design we have slightly increased the radius of curvature of the secondary from its nominal value of 200 to 201.5 mm (while keeping the mirror pair concentric) in order to induce a small amount of 3rd order astigmatism that balances the 5th order astigmatism to produce nearly zero astigmatism at the center of the field, as was suggested by Offner.[9] We have also fabricated a central hole in the Offner secondary to reduce thermal background due to stray light from the telescope primary hole. Since the Offner primary produces an image of the telescope primary slightly in front of the Offner secondary, this adjustment moves the Offner secondary closer to this image and improves its function as a Lyot stop. Figure 2 presents spot diagrams at the telescope focal plane and at the reimager focal plane showing the distribution of light at the central field position and at the corners and edges of the ASTROCAM field of view. Even at the corners of the field the telescope aberrations are small
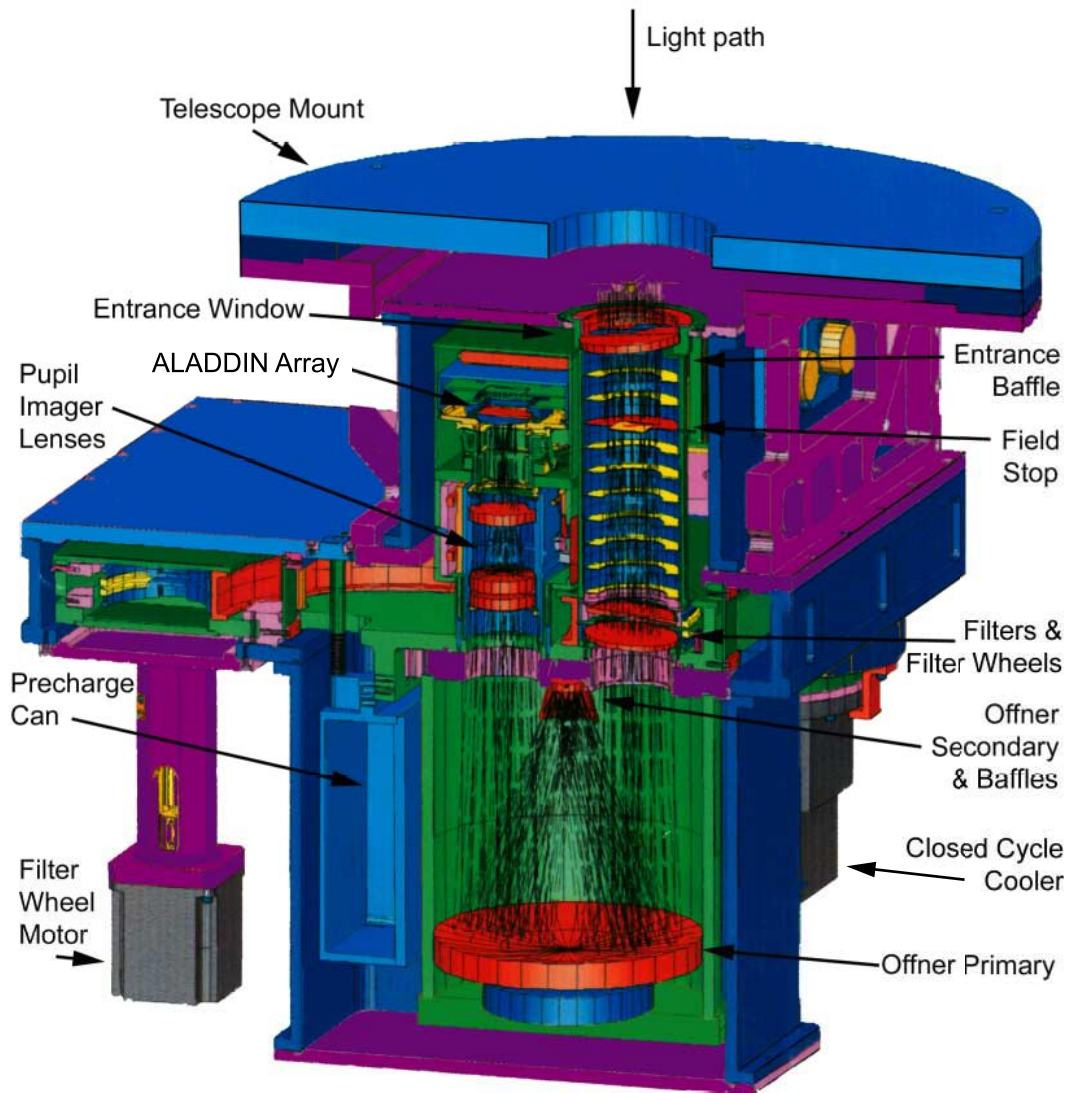
Figure 1. A CAD drawing of ASTROCAM in pupil imaging mode. The pupil imaging optics are translated out of the beam during normal operation.

compared with the seeing and diffraction effects discussed at the beginning of this section and there is negligible additional degradation due to the Offner: at the outermost corner the spot size of the reimager optics is 12 μm. Distortion is less than 0.01%.

Longward of 3 μm, diffraction effects begin to become noticeable in comparison to the seeing. If the Offner spherical mirrors were figured perfectly, they would yield a wavefront error of $\lambda/47$ at 3 μm at the corner of the field of view due to astigmatism, which is more than sufficient to be diffraction limited. We toleranced the alignment and surface quality of the mirrors to maintain the diffraction limit at this wavelength.

If the aperture stop of an optical system (here the camera Lyot stop) is situated in the back focal plane of that part of the system which precedes it, the entrance pupil is at infinity, all the principal rays in object space will be parallel to the axis, and the system is said to be telecentric on the object side. Similarly, if the aperture stop of a system is situated in the front focal plane of that part of the system which follows it, the exit pupil
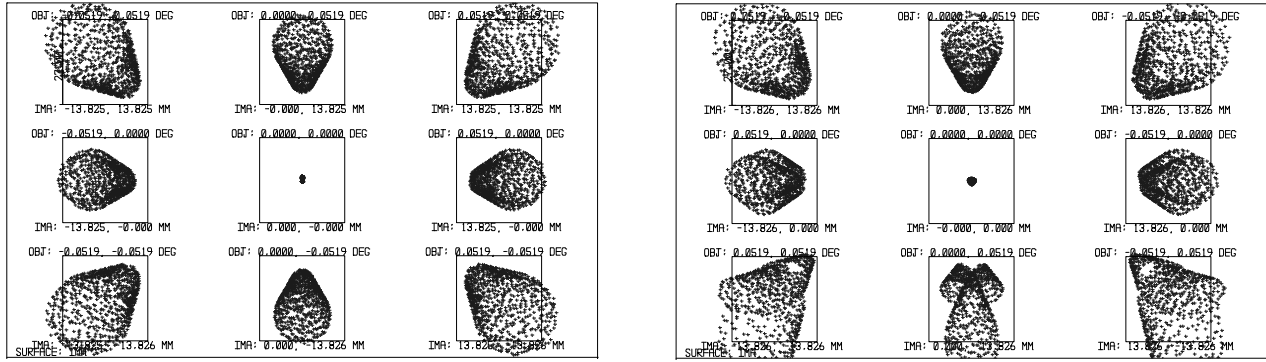
Figure 2. Spot diagrams at the center, edges, and corners of the 1.55-m telescope focal plane (left) and the ASTROCAM Offner reimager focal plane, relative to the 27 μm $\times$ 27 μm ALADDIN pixels (represented by boxes).
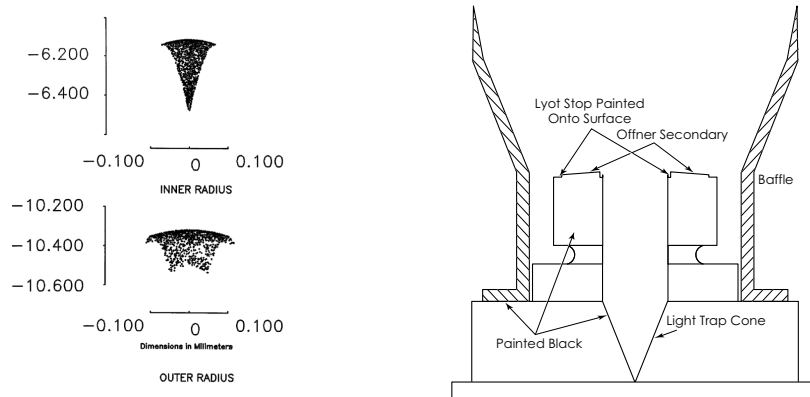
Figure 3. (Left) Spot diagrams at the inner and outer edges of the ASTROCAM Offner secondary. Scale is in millimeters. (Right) The Offner secondary mirror functions as the system Lyot stop.

(the image of the stop in image space) is at infinity, the principle rays in image space will be parallel to the axis, and the system is said to be telecentric on the image side.[10]   An optical system with telecentricity on the image side has several desirable characteristics for astrometry and photometry.[11]   In particular, since the beam bundles are normal to the array, telecentricity on the image side means that any defocus will not result in a change of image scale, a very useful property for astrometry. Since the Offner secondary is at the Offner primary's sagittal plane focal point and only about 3 mm from the tangential plane focal point, it can function as a Lyot stop, and render the system nearly telecentric: for an image taken 0.1 mm out of focus, the angualr separation of the image centroids of two point sources separated by the width of the array changes by less than 0.003 arc seconds compared with an in-focus image. The spot diagram in Figure 3 (left) shows the distribution of light from point sources at the inner and outer radii of the telescope primary at the position of the Offner secondary. The secondary outer diameter was set to the telescope primary image on the secondary, and the inner diameter was set by the telescope sky baffle. Inner and outer annular edges about equal in size to that of the blur spots on the secondary were cut away to allow accurate masking with black paint. Absorptive baffles and a black central cone provide additional stray light rejection (Fig. 3, right) at the Lyot stop. In addition, the system is baffled both before and after the field stop on the input side, with a central baffle vane between the input and output beams, and at several positions along the output beam (see Figures 1, 4, and Section 4).

The CaF$_2$ window and filters, the only transmissive optics in the design, were tilted by 5° in opposite directions to eliminate ghosts images and located as far as possible from the field stop so that any dust particles on the filters are not in focus. ASTROCAM is currently equipped with the Z, J, H, K, K', K-long, and L'

standard astronomical broadband filters and narrowband filters centered on and off the [Fe II]1.64 μm, 1-0 and 2-1 S(1)lines of H_2 at 2.12 and 2.25 μm, the hydrogen Brγ line at 2.16 μm, and the polycyclic aromatic hydrocarbon feature at 3.28 μm.

3.3. The pupil imager

If the telescope's primary mirror is not properly imaged and aligned on the Lyot stop, warm radiation from outside the primary's outer edge and from inside its inner edge will be transmitted through to the focal plane. In order to examine the quality and alignment of this image, we designed and fabricated pupil-imaging optics (the three elements labeled "pupil imager lenses" in Figure 1) that can be slid into the optical path to image the Lyot stop and pupil onto the ASTROCAM focal plane array. The two closely-spaced elements constitute an achromat, made from BaF_2 (first element) and LiF (second element). This achromat transfers the (virtual) image, located approximately at infinity as stated in the telecentricity discussion above, of the Lyot stop formed by the image side of the Offner primary to the ASTROCAM focal plane array. The Offner primary contributes substantial spherical aberration to this image. To correct this off-center spherical aberration, the third element is an off-center segment of a Schmidt corrector plate, placed at the image formed by the achromat of the Offner's field stop. This is the right place to put the corrector since the Offner's field stop is located in the same plane as the center of curvature of the Offner primary. Using the resulting good image through one of the thermal filters, alignment of the telescope primary's image on the Lyot stop can be accurately checked for thermal radiation leakage past the stop and corrected by improving the alignment.

The optical design included the calculation of the positioning of the optics at room temperatue and at the 77 K operating temperature. The system was then built to specified tolerances so that minimal alignment during fabrication was necessary.

4. MECHANICAL DESIGN AND FABRICATION

The design of the cryostat and optical bench layout is shown in detail in Figure 1. The cryostat utilizes a box configuration due to its inherent stability (Figure 1) and the cold shielding is done by enclosing the optics in a sequence of enclosures. The Offner relay was fabricated as an enclosed, aligned cylindrical assembly with circular input and output openings (Figure 4). In order to minimize weight and volume, the 17 2.75-inch filters and separate blocker are mounted in an enclosure housing a pair of 18-inch diameter filter wheels (Figure 5, left) that circumscribes the entire input and output optical train. The rest of the optical bench consists of the cryostat window, cylindrical field stop and baffle tube, pupil imaging optics and its housing, and the detector and its housing (Figure 6).

The Offner optics and structure were produced from same melt, heat treated, and stress relieved aluminum alloy in order to provide a passively athermalized optical system. A hole and inner and outer Lyot stop edges were machined into the center of the secondary, and the inner diameter, outer diameter, and true positioning of the optical surface with respect to the physical mirror, were all held to very tight tolerances. The system's image quality and stability down to cryogenic temperatures have been ensured by the application of a number of material processing and thermal cycling steps. In order to meet our overall system level wavefront requirements both the mirrors were diamond turned and polished as bare aluminum mirrors. This process is more time consuming than the traditional electroless nickel coated aluminum mirror manufacturing flow. However, the elimination of the nickel layer avoids CTE mis-match between the nickel and the aluminum, and thus eliminates any wavefront errors created by the bimetallic bending of the mirror as it cools down to its operational temperature and significantly improves the system's thermal stability. The reflectivity of the electrolytic gold-coated mirrors was 0.96 at 1 μm and almost 0.99 at 5 μm. An interferogram depicting the finished surface figure obtained in the bare aluminum primary mirror is presented in Figure 4 (bottom, right). The entire mirror shows a surface figure error of 0.22 waves peak-valley (at $\lambda = 0.6$ mm). This represents an upper limit to the surface figure error over the small sub-aperture of the mirror surface that is used.

Alignment of the Offner assembly was done using a combination of precision mechanical placement and interferometric optical alignment. Since the Offner reimager is composed of a pair of concentric spherical mirrors, optimum alignment can be achieved by adjusting only the mirror pair's centration and separation. The
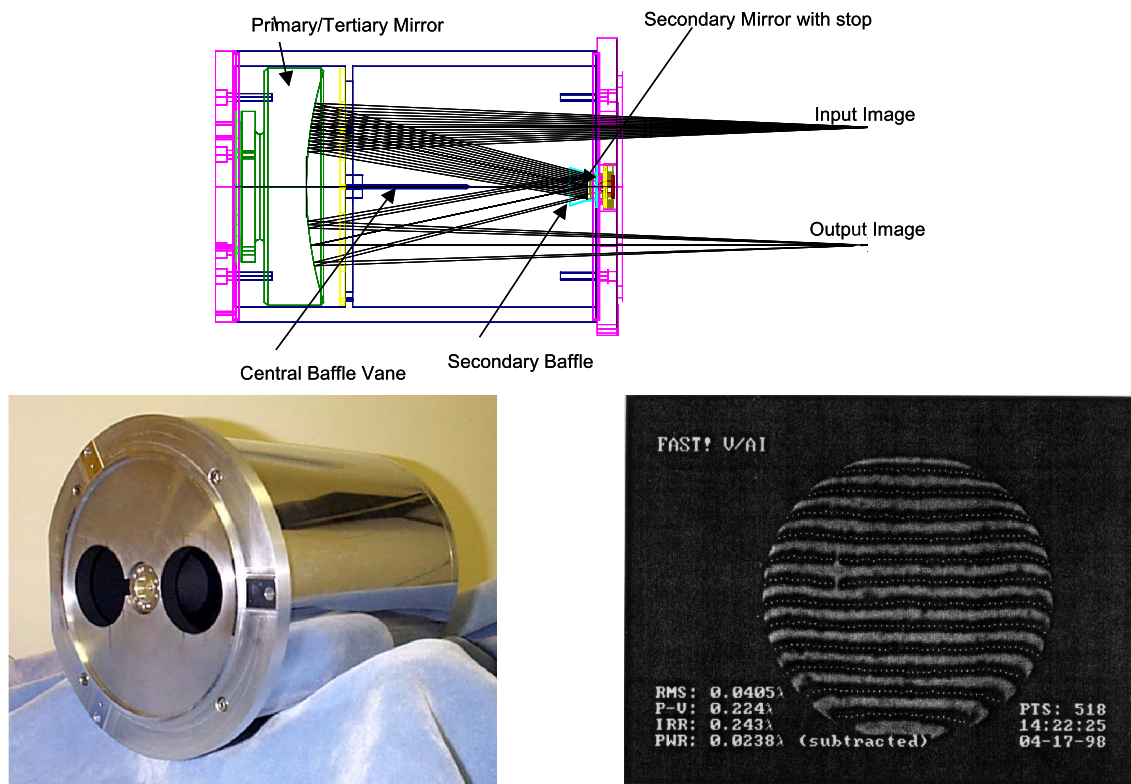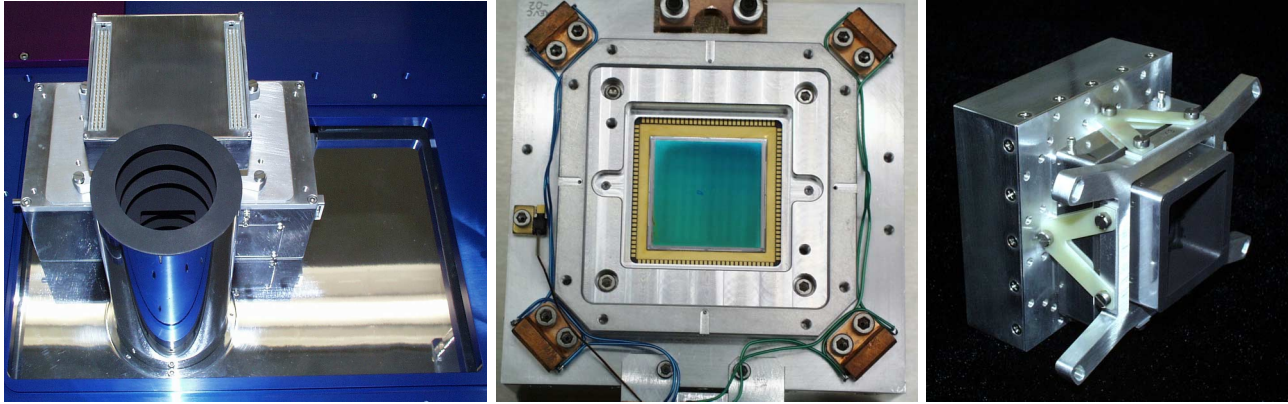
Figure 4. (Top) Optomechanical schematic of the mounted Offner optics. (Bottom, left) Offner optics housing. (Bottom, right) Interferogram of the Offner primary ($\lambda = 0.6$ μm).
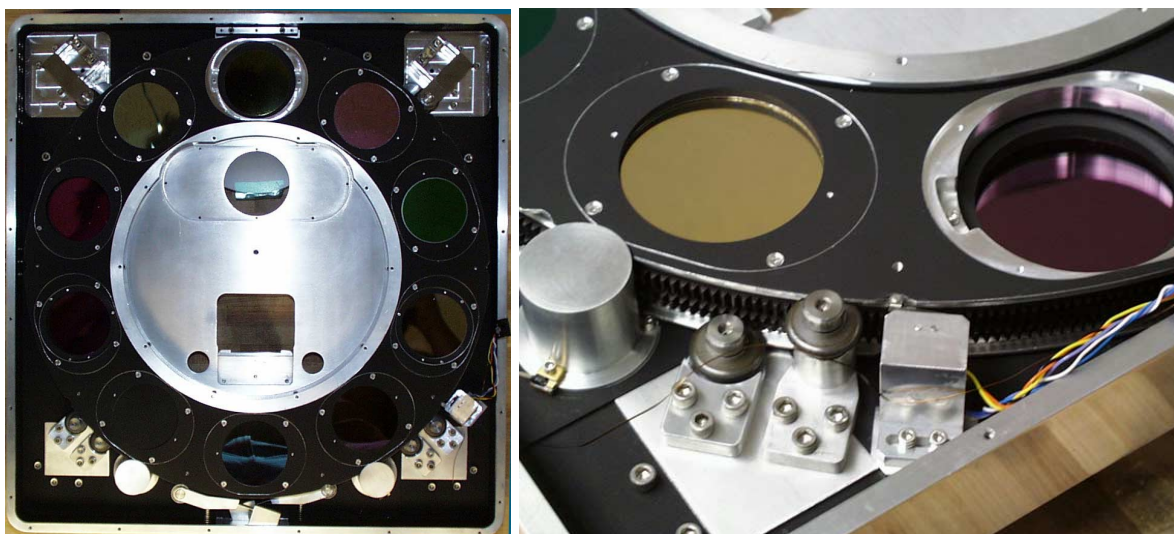
Figure 5. (Left) Photograph of the filter wheel assembly. (Right) Photograph of the double filter wheel gear mechanism showing vespel rollers and housed pinion gears.

Figure 6. (Left) Photograph showing the assembly of the baffle tube, field stop, pupil imager housing, and detector housing. (Middle) Photograph of ALADDIN science array, heaters, and temperture sensors. (Right) Detector baffle, V-shaped fiberglass truss, and Faraday shield.

secondary was fabricated with its optical center well aligned with its substrate, so by rotating the secondary mirror on its mounting plate, use of an air bearing and dial indicator allowed us to center the optical surface on the mounting plate. The centration of the primary mirror on its mount can then be adjusted interferometrically using a point source generated by a laser unequal path interferometer (LUPI) at the position of a ball bearing whose axis of motion is aligned parallel to that of the air bearing cylinder and dial indicator and interferometer. The primary mirror mounted to the Offner housing is then centered mechanically onto the secondary using the dial indicator and the now concentric air bearing cylinder. This alignment process greatly facilitated the final LUPI interferometric adjustment of the mirror separation performed using retroreflection by a concave mirror of a point source sent from the Offner input to the output. The resulting average system level wavefront error of the Offner (measured over 13 field points) is 0.126 waves RMS and 0.551 waves peak-valley. These measurements include aberrations which result from design residual errors and which cannot be removed even with a perfect system, optical fabrication, and optical alignment. A photograph of the final enclosed Offner system is shown in Figure 4 (left, bottom). The exterior of the housing has been polished to a highly specular finish in order to minimize the emissivity of the system.

The dual filter wheel assembly is shown in Figure 5. Since the optical system occupies the central region of the filter wheel assembly, both the mechanical support (by two vespel and two spring loaded rollers) and the rotation (by a pinion gear) of each filter wheel are done at the outer edge. The spring loaded rollers accommodate differential contraction during cooldown. Limit switches are used to attain the correct stopping locations of the filter wheel. Each filter is mounted in an individual baffled cell, with easy access through plates in the filter wheel housing and vacuum jacket.

The pupil imager lenses were mounted using three axial bumps and a three finger spring for axial support and two radial bumps with a radial leaf spring in order to achieve the necessary radial and axial position tolerances ($\sim$ 0.001 inch) without breaking during cooldown. Both the filter wheels and the pupil imager are actuated with warm stepper motors, with light-tight vacuum feedthroughs.

The ALADDIN array detector, mask, and baffle (Figure 6, right) are attached to the Faraday shield that houses the fan-out boards to the cold electronics on a V-shaped fiberglass truss (for thermal resistance) with curved slotted holes, shoulder screws and shims to allow changes in alignment if necessary. Surrounding the detector are four copper block heaters, a brass-mounted temperature sensor, and a cold strap connector (copper) and bracket (aluminum) (Figure 6, middle). There is also a temperature sensor on the detector cold finger.

The cryostat and aluminum vacuum jacket were designed to maximize the ease of access and assembly. The lower part of the vacuum jacket can be removed to access the Offner relay without disconnecting anything as there are no penetrations or feedthroughs in that area. The upper part of the vacuum jacket can also be removed

after disconnecting the pupil imager drive and detector cables. The two filter wheel motors and the closed cycle cooler mount to the bottom of the center portion of the vacuum jacket and never need to be removed during any repair as full access is available without removing the cold structure from this center part of the vacuum jacket. Only the pupil motor needs to be disconnected for a complete service of any part.

The CTI model 1050 closed cycle cooler and model 1020R compressor maintain the cold structure at 77 K and cool the detector to its operating temperature of 30 K. The closed cycle cooler is oriented with the cold finger parallel to the telescope optical axis so the movement of the piston will not cause image movement. The cooler is mounted to the cryostat using a tuned isolator made of a welded metal bellows surrounded by a machined Buna rubber vacuum ring. The cooler's cold finger is connected to the cold structure via a multi-layer copper sheet strap. A liquid nitrogen precharge can with 24 hour hold time is used to speed cool down.

5. ELECTRONICS

The ASTROCAM electronics system is composed of four major subsections. The user interfaces with the system via the "X" User Interface (XUI) and instrument control programs running in the VME64 control subsystem. This subsystem generates digital clock signals that are transmitted to the cryostat mounted readout electronics subsystem where they are translated to proper analog clock drive voltages. The array outputs are preamplified, digitized and returned back to the VME64 control subsystem. The cryostat mounted electronics are powered by a separate low noise power supply. The cryostat electronics subsystem consists of integrated array mounted fanout boards, cryostat cables, and thermal light-tight feedthroughs. The instrument motor and temperature control subsystem consists of an ethernet-based serial port server communicating with the servo motors and temperature controller. The electronics are similar to those developed for the Infrared Telescope Facility SpeX instrument.[12]

The VME64 chassis houses a Themis UltraSPARCIIi with input and output via fiber and 100 base-TX ethernet links. This computer provides outside access and control to the two Ixthos IXZ4444 quad SHARC DSP boards. One DSP runs a realtime program that generates 32 bits of digital clock pattern that is output to the fibre channel link. Another DSP on the same board receives the digitized pixel values for the top two quadrants of the array. A separate fibre channel plus DSP board receives the digitized pixel values for the bottom two quadrants of the array. Each fiber interface to the cryostat mounted readout electronics is a class 1, 850 nm bi-directional laser link carried on two 62/150 μm multimode fiber cables with ST connectors.

A 63HP Eurocard chassis houses a set of custom low noise array readout electronics that provides 32 channels of analog clock drivers and 32 channels of preamplifiers and 16 bit 2 MHz analog to digital converters for the ALADDIN array. Connection to the internal cryostat electronics is made through two 61 pin low capacitance cables. These cables are fabricated from multiple coaxial cables. They mate with the two cryostat mounted hermetic connectors. A specially modified HP 66000 series system power supply supplies the power for the cryostat mounted electronics and the Animatics servo motors. The low noise array supplies are HP power modules; the fan and servo motor supplies are linear supplies. A 16 pin power cable connects to a chassis mounted connector providing +5 V, +15 V, -15 V and +24 V DC supply power for the cryostat mounted electronics. Figure 7 is a schematic diagram of the readout electronics.

A separate utility box is attached to the side of the 63HP chassis that breaks out two cables from the temperature controller/ethernet motor control chassis, which houses a Lakeshore model 330 cryogenic temperature controller as well as a Lantronix ethernet serial port server. An ethernet interface input allows the Themis UltraSPARCIIi/VME64 computer to communicate with the Lakeshore model 330 temperature controller and the three Animatics servo motors via the Lantronix serial server. The utility cable carries the signals for temperature control to the temperature diode and heater resistors. It connects to the cryostat temperature hermetic connector. A communication cable carries the three sets of RS-232 signals (for the servo motors) to the junction box.

5.1. Multiple subarray readout capability

To allow readout of the full frame (1024 × 1024) at backgrounds as high as those in the narrowband 3 μm filters, the ASTROCAM electronics were designed to sustain a full frame single read rate of 20 Hz. Readout
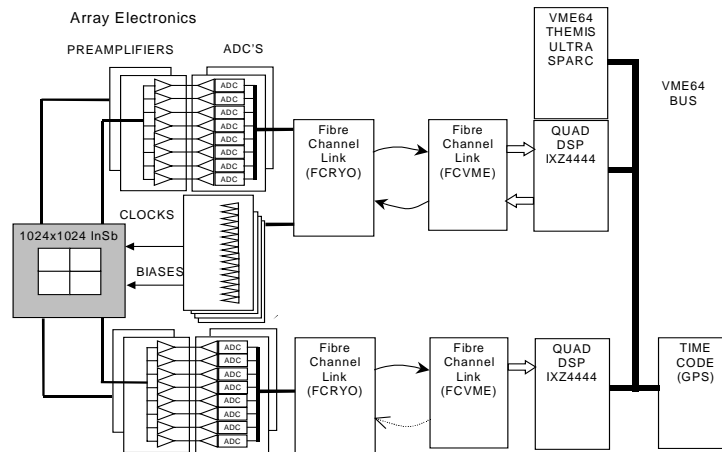
Figure 7. Schematic diagram of the ASTROCAM readout electronics.

of a full frame array with double-correlated sampling can be done in 0.19 seconds. In order to enable L'-band observations, for which the thermal background saturates the array at the fastest rate at which the entire array can be read out, a multiple subarray readout capability was designed. A subarray readout mode was implemented in the array control electronics, where up to 14 subarrays can be read out and stored. Software was developed to generate the appropriate clocking patterns to minimize the time overhead from the "ghost" readouts of the mirrored subarray on the remaining quadrants (resulting from the architecture of the ALADDIN III multiplexer). The clocking is further complicated by the fact that the multiplexer outputs 8 columns per quadrant.

The system takes the subarray size(s) and position(s) as input from the graphical user interface on the VME64 Themis UltraSPARCII computer. The program determines the necessary clocking sequence and row patterns and downloads these sequences and patterns to the Analog Devices SHARC DSP on the VME64 IXZ4444 board which does the clocking function for the system. When the DSP is commanded to read out the array, it proceeds to execute the sequences in deterministic, real-time.

Array readout was accomplished for all four quadrants simultaneously using global reset and readouts. Each row's clocking patterns were pre-determined based on the subarray positions. The minimum readout time for a particular subarray is dependent on its position on the array. For a double readout (reset, pedestal read and signal read) of a single 32×16 pixel subarray, the minimum readout time achieved was 1.3 msec at position [0,0], 4.1 msec at position [256,256] and 6.3 msec at position [448,448]. Readout times for multiple subarrays are generally shorter than simple multiplication of the single subarray times. For example, readout of these three subarrays takes only 7.1 msec since some of the fixed overhead is shared by the three subarrays.

6. SOFTWARE

The ASTROCAM software system was modeled after the IRTF SpeX instrument. Upon initialization, low-level control software is downloaded from the SPARC into the DSP card to control the basic clocking, exposure timing, and data acquisition. After an image is acquired, it is transferred through a shared memory buffer to the host SPARC. Time-critical routines are written in SHARC assembler; all control routines except for the filter wheel control software are in C. Two SHARC DSP chips each control one-half of the array to optimize data flow; one SHARC handles the DSP/SPARC communication. The low-level software is quite flexible, implementing multiple windows during readout along with single read, Fowler sampling, and pedestal read modes. Co-adding is done in DSP hardware, and multiple frames can be created from software looping in the DSP card. Most of the operating voltages are set with remotely programmable DACs, so changing bias or setpoints is performed with small software scripts.

The host SPARC runs four tasks: an interface task (IC) to the DSP card; a "tcl/tk" task (MOTORPANEL) to control the filter wheels; an image display task (DV) for standalone image display on the SPARC; and a user-interface (XUI) to accept user commands such as for file naming and exposure setup. Both DV and XUI use the "gtk" library for window support.

The paragraphs above describe the instrument stand-alone mode, storing frames on a local hard drive and transferring the frames via Berkeley sockets to the DV program to display the images on a local graphics card. In the Naval Observatory Flagstaff Station (NOFS) software environment, the DV program is not executed; instead, its socket interface is utilized by an existing NOFS data acquisition computer to transfer frames from the SPARC to be displayed and archived. A second socket interface is implemented through the MOTORPANEL task to send and receive commands and status information. With 100 base-T ethernet, image transmission is less than one second. The NOFS data acquisition computer uses a combination of C, Fortran and Forth for instrument control, and talks to both a telescope computer with sockets and a user console with X-windows. Images acquired by ASTROCAM are transmitted to the NOFS computer in FITS format, where they are modified to insert telescope status information before final storage and display on the user console.

The NOFS instrument control software gives the user a choice of dither patterns, makes region-of-interest window selection easier, provides standard stars for photometric projects, does automated reacquistion of guide stars after dithered moves, applies flatfielding and image subtraction to displayed images, generates contour plots and basic photometry of objects within a frame, and in general attempts to make the observer as efficient as possible in data collection and real-time analysis. For final processing, scripts have been developed in IRAF to automatically archive the data, apply linearization correction to all raw frames, search through the nightly frames to create master flats, flatfield and sky subtract the raw frames, and also insert registration information into the FITS headers of those fields that belong to the observatory parallax program.

In the near future, we will be implementing a high-speed time series mode, where only regions of interest from each data frame are collected and saved with buffered writes so that minimal deadtime occurs. We will also be performing real-time shift-and-add processing to obtain the sharpest images possible without additional hardware.

7. INSTRUMENT TESTS AND FIRST RESULTS

ASTROCAM has been operational at USNO since "first light" during late August 1999 (Figure 8, left). In this section we present images made with the pupil imager, upper limits on distortion, estimates of faint star astrometric precision, and examples of wide field tri-color images obtained with ASTROCAM. We also report our 3σ point source sensitivity in 10 minutes of approximately 17th magnitude through the K' filter in good seeing.

7.1. Pupil images

Figure 8 (right) shows sharp pupil images of the Lyot stop with the telescope at zenith and at 45° north and south, and 45° east and west of zenith along constant declination. These images show the expected thermal radiation from the telescope secondary spider support and the three seismic clips at the outer edge of the primary. They also show narrow crescents of warm radiation "leaking" past the outer edge of the Lyot stop that change with telescope position. Subtraction of the images shows that the spiders, seismic clips and crescents move along gravity vectors with respect to the array that are consistent with either small tilt motion of the telescope secondary or of the telescope tailpiece. Corrective steps are planned.

7.2. Test for distortion

To test for optical distortion in the 6.2 arc minute × 6.2 arc minute field of view of ASTROCAM, we imaged four fields through the J-band filter in the SDSS astrometric calibration region E[13] on the night of February 2, 2001, with clear skies and 1.6 arc second seeing. The integration time for each field was 30 seconds × 6 exposures. For each ASTROCAM field, frames were flat-fielded using dome flats, stars were extracted using DAOPHOT as implemented in IRAF, and then a linear plate solution was generated using the SDSS calibration field stars as the reference frame to produce a mean fit for the field with proper rotation, offset and scaling.
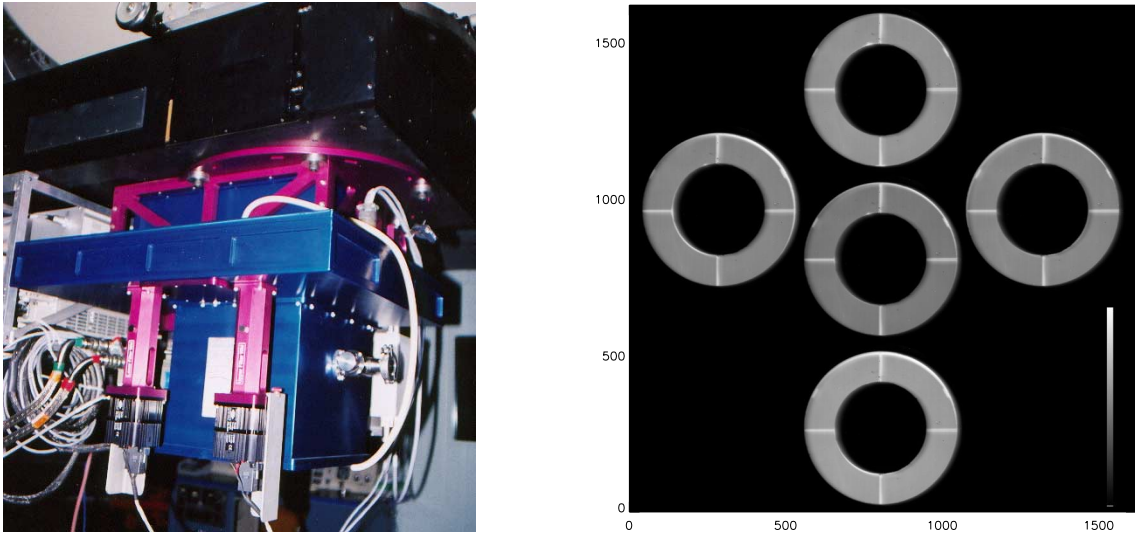
Figure 8. (Left) ASTROCAM mounted on the USNO 1.55-m astrometric telescope. (Right) A narrow band 3.16 μm montage of images of the Lyot stop taken with the pupil imaging optics. The telescope is pointed at zenith (central image) and at 45° north and south and 45° east and west of zenith along constant declination. North is up, east is to the left, and the x and y scales are in pixel units.
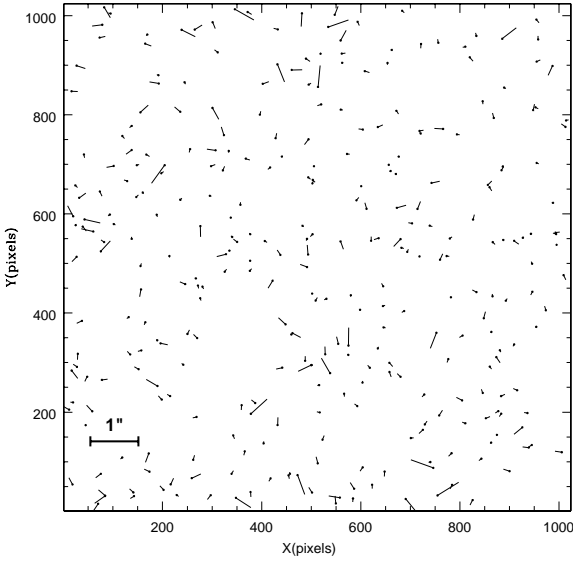
Figure 9. Residuals of linear plate solutions of ASTROCAM fields using astrometic SDSS stars as the basis for the fits. The scale is in pixel units.
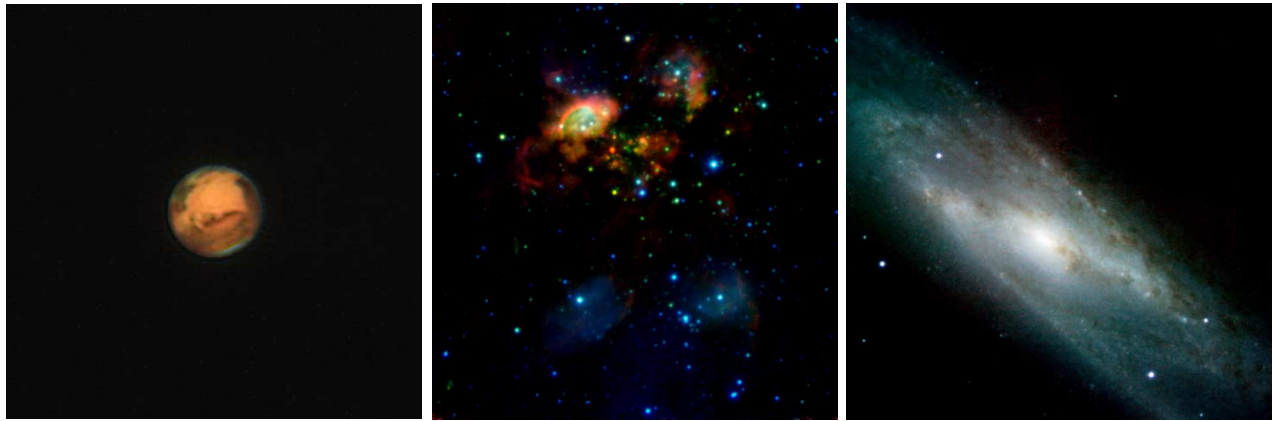
Figure 10. (Left) Tri-color 1.57 μm, 2.16 μm, and 3.28 μm narrowband image of the 2001 opposition of Mars. (Middle) Tri-color J, K, 3.16 μm ASTROCAM image of the W3OH star formation region. (Right) Tri-color J, H, K-band ASTROCAM image of the dusty galaxy NGC 253.

The residuals between the ASTROCAM positions and the SDSS positions were then tabulated as a function of x,y position on the detector. Figure 9 shows a dot symbol plotted at the location of every star on the array and a bar showing the residual magnitude and direction of the residual offset. The measurement bar indicates the length of an arrow if one arcsec of residual were present. The mean residual is under 100 mas. About half of this residual is expected to be due to errors in the SDSS reference frame and the highest residuals were found for the faintest stars where the most centroiding error is to be expected. The lack of an apparent systematic trend in the plot indicates that no measurable distortion is present in the field of view.

7.3. Astrometric precision on faint stars

Since September of 2000 ASTROCAM has been employed in a program to determine parallaxes and proper motions of L- and T-dwarfs. While not an ideal test of the ultimate astrometric performance of ASTROCAM, the IR parallax program results can give a good indication of astrometric quality in an application requiring long-term astrometry of faint stars. For approximately 12 nights each lunation, ASTROCAM is used at the 1.55-m telescope obtaining observations near the meridian of parallax star fields when the seeing is less than or equal to 2.5 arcsec FWHM and through any cloud conditions which do not totally prevent observations. There are currently 41 stars on the program, split approximately evenly between L- and T-dwarfs. Of these, data for 16 fields have so far been reduced; eight L-dwarfs and eight T-dwarfs. The L-dwarfs are observed in the H-band with magnitudes ranging from 13.8 to 15.9 and with reference frame stars ranging from 12.0 to 16.5. The T-dwarfs are observed in the J-band with magnitudes ranging from 14.1 to 16.0 and with reference frame stars ranging from 13.0 to 16.8. There are from 6 to 16 reference frame stars used for each field, randomly scattered over the entire ASTROCAM FOV. Observations always consist of three dithers, separated by 10 arc seconds, and, due to the faintness of the stars, total integration times of from 30 to 90 minutes depending on the field and sky conditions. The data are linearized and flattened using previous calibration sets and a sky frame, formed from the three dithers, is subtracted. The stellar positions on each such processed frame are then measured with 2-D Gaussian fits.

Astrometric standard errors of unit weight for all reference frame stars on all three dithers on nights with seeing of 1.6 arcsec or less are typically 6 mas, with no statistically significant differences between X and Y (which are aligned with right ascension and declination) nor between observations taken in the J- or H-bands. We note, however, that the typical astrometric standard errors of unit weight reported here should be regarded only as upper limits to those ultimately achievable with ASTROCAM. For instance, while there is relatively little differential color refraction at J or H, the 10 to 30 minute per dither exposures (necessitated by the relatively small aperture telescope used) are guided by an autoguider operating at optical wavelengths. Hence

the differential color refraction smear between the optical and IR is effectively transferred to the IR images. Differential astrometry of bright stars with short exposures and taken under ideal seeing and background conditions would likely yield astrometric results significantly better than the 6 mas measured in our program work.

Lastly we present three tri-color images taken with a range of dither sizes and with both broadband and narrowband filters of planetary, galactic, and extragalactic fields in Figure 10. A monthly monitoring program of a flux limited (at 60 μm) sample of dusty galaxies including NGC 253 (Figure 10, right) is being carried out at K' with ASTROCAM to search for dust obscured supernovae in galactic nuclei.

ACKNOWLEDGMENTS

REFERENCES

1. D. G. Monet, C. C. Dahn, F. J. Vrba, H. C. Harris, J. R. Pier, C. B. Luginbuhl, and H. D. Ables, "U.S. Naval Observatory CCD parallaxes of faint stars. I - Program description and first results," *Astron. J.* **103**, pp. 638–665, 1992.
2. C. C. Dahn, H. C. Harris, F. J. Vrba, H. H. Guetter, B. Canzian, A. A. Henden, S. E. Levine, . C. B. Luginbuhl, A. K. B. Monet, D. G. Monet, J. R. Pier, R. C. Stone, R. L. Walker, A. J. Burgasser, J. E. Gizis, . J. D. Kirkpatrick, J. Liebert, and I. N. Reid, "Astrometry and photometry for cool dwarfs and brown dwarfs," *Astron. J.* **124**, pp. 1170–1189, 2002.
3. A. M. Fowler, J. B. Heynssens, I. Gatley, F. J. Vrba, H. D. Ables, A. Hoffman, and J. Woolawy, "ALADDIN, the 1024 × 1024 InSb array: Test results," in *Infrared Detectors and Instrumentaion for Astronomy*, A. M. Fowler, ed., *Proc. SPIE* **2475**, pp. 27–33, 1995.
4. D. C. Murphy, S. E. Persson, M. A. Pahre, A. Sivaramakrishnan, and S. G. Djorgovski, "An infrared camera for the Palomar observatory 60-inch telescope," *Publ. Astron. Soc. Pac.* **107**, pp. 1234–1242, 1995.
5. J. R. Graham and R. R. Treffers, "An infrared camera for Leuschner Observatory and the Berkeley Undergraduate Astronomy Lab," *Publ. Astron. Soc. Pac.* **113**, pp. 607–621, 2001.
6. V. N. Mahajan, "Line of sight of a aberrated optical system," *J. Opt. Soc. Amer.* **2**, pp. 833–846, 1985.
7. H. C. Harris and F. J. Vrba, "Seeing measurements and observing statistics at the U.S. Naval Observatory, Flagstaff Station," *Publ. Astron. Soc. Pacific* **104**, pp. 140–145, 1992.
8. A. Offner, *Unit Power Imaging Catoptric Anastigmat*, United States Patent 3,748,015, July 24, 1973.
9. A. Offner, "New concepts in projection mask aligners," *Optical Engineering* **14**, pp. 130–132, 1975.
10. M. Born and E. Wolf, *Principles of Optics, Sixth Edition*, Pergamon Press, Oxford, United Kingdom, 1986.
11. J. Rayner, M. Shure, D. W. Toomey, P. Onaka, A. Denault, W. Stahlberger, D. Watanabe, K. Criez, L. Robertson, D. Cook, and M. Kidger, "Design of a new 1-5.5 μm infrared camera for the NASA Infrared Telescope Facility," in *Infrared Detectors and Instrumentation*, A. M. Fowler, ed., *Proc. SPIE* **1946**, pp. 490–501, 1993.
12. P. M. Onaka, A. J. Denault, D. Y. Watanabe, G. K. Ching, D. W. Toomey, and J. T. Rayner, "The REDLINE multiple array controller for SpeX," *Proc. SPIE* **3354**, pp. 139–150, 1998.
13. R. C. Stone, J. R. Pier, and D. G. Monet, "Improved astrometric calibration regions along the celestial equator," *Astron. J.* **118**, pp. 2488–2502, 1999.